



Deposited via The University of Leeds.

White Rose Research Online URL for this paper:

<https://eprints.whiterose.ac.uk/id/eprint/87063/>

Version: Accepted Version

Article:

Mobilia, M (2015) Nonlinear q-voter model with inflexible zealots. *Physical Review E: Statistical, Nonlinear, and Soft Matter Physics*, 92. 012803. ISSN: 1539-3755

<https://doi.org/10.1103/PhysRevE.92.012803>

Reuse

Items deposited in White Rose Research Online are protected by copyright, with all rights reserved unless indicated otherwise. They may be downloaded and/or printed for private study, or other acts as permitted by national copyright laws. The publisher or other rights holders may allow further reproduction and re-use of the full text version. This is indicated by the licence information on the White Rose Research Online record for the item.

Takedown

If you consider content in White Rose Research Online to be in breach of UK law, please notify us by emailing eprints@whiterose.ac.uk including the URL of the record and the reason for the withdrawal request.

Nonlinear q -voter model with inflexible zealots

Mauro Mobilia¹

¹*Department of Applied Mathematics, School of Mathematics, University of Leeds, Leeds LS2 9JT, U.K.**

We study the dynamics of the nonlinear q -voter model with inflexible zealots in a finite well-mixed population. In this system, each individual supports one of two parties and is either a susceptible voter or an inflexible zealot. At each time step, a susceptible adopts the opinion of a neighbor if this belongs to a group of $q \geq 2$ neighbors all in the same state, whereas inflexible zealots never change their opinion. In the presence of zealots of both parties the model is characterized by a fluctuating stationary state and, below a zealotry density threshold, the distribution of opinions is bimodal. After a characteristic time, most susceptibles become supporters of the party having more zealots and the opinion distribution is asymmetric. When the number of zealots of both parties is the same, the opinion distribution is symmetric and, in the long run, susceptibles endlessly swing from the state where they all support one party to the opposite state. Above the zealotry density threshold, when there is an unequal number of zealots of each type, the probability distribution is single-peaked and non-Gaussian. These properties are investigated analytically and with stochastic simulations. We also study the mean time to reach a consensus when zealots support only one party.

PACS numbers: 05.40.-a, 02.50.-r, 89.75.-k, 89.65.-s

I. INTRODUCTION

The voter model (VM) [1] is one of the simplest and most influential examples of individual-based systems exhibiting collective behavior. The VM has been used as a paradigm for the dynamics of opinion in socially interacting populations, see *e.g.* [2, 3] and references therein. The classical, or linear, VM is closely related to the Ising model [4] and describes how consensus results from the interactions between neighboring agents endowed with a discrete set of states (“opinions”). While the VM is one of the rare exactly solvable models in non-equilibrium statistical physics, it relies on oversimplified assumptions such as perfect conformity and lack of self-confidence of all voters. This is clearly unrealistic as it is recognized that members of a society respond differently to stimuli: Many exhibit conformity while some show independence, and this influences the underlying social dynamics [5–7]. In order to mimic the dynamics of socially interacting agents with different levels of confidence, this author introduced “zealots” in the VM [8–11]. Originally zealots were agents favoring one opinion [8, 9]. The case of inflexible zealots whose state never changes was then also studied [10], and the influence of committed and/or independent individuals was considered in various models of opinion dynamics [11, 12]. Recently, authors have investigated the effect of zealots in naming and cooperation games, and even in theoretical ecology [13].

In recent years, many versions of the VM have been proposed [2]. A particularly interesting variant of the VM is the two-state nonlinear q -voter model (q VM) introduced in [14]. In this model q randomly picked neighbors may influence a voter to change its opinion. When $q = 2$, the q VM is closely related to the Sznajd model [15–17]

and to that of Ref. [18]. The properties of the q VM have received much attention and there is a debate on the expression of the exit probability in one dimension [18–20].

Here, we investigate a generalization of the nonlinear q VM, with $q \geq 2$, in which a well-mixed population consists of inflexible zealots and susceptible voters influenced by their neighbors. As a motivation, this parsimonious model allows to capture three important concepts of social psychology [6] and sociology [5]: (i) conformity/imitation is an important social mechanism for collective actions; (ii) group pressure is known to influence the degree of conformity, especially when a group size threshold is reached [7]; (iii) the degree of conformity can be radically altered by the presence of some individuals that are capable of resisting group pressure [6, 7]. Here, the q VM mimics the process of conformity/imitation with group-size threshold, whereas zealots are independent agents that resist social pressure and can thus prevent to reach unanimity.

In this work, we study the fluctuation-driven dynamics of the two-state q VM with zealots in finite well-mixed populations and shed light on the deviations from the mean field description and from the linear case ($q = 1$). We find that below a zealotry density threshold the probability distribution is bimodal instead of Gaussian and, after a characteristic time, most susceptibles become supporters of the party having more zealots. When both parties have the same small number of zealots, susceptibles endlessly swing from the state where they all support one party to the other with a mean switching time that approximately grows exponentially with the population size.

In the next section we introduce the model. Sections III and IV are dedicated to the mean-field description and to the model’s stationary probability distribution. In Sec. V and VI we discuss the long-time dynamics and the mean consensus time when there is one type of zealots. We summarize our findings and conclude in Sec. VII.

*Electronic address: M.Mobilia@leeds.ac.uk

II. THE q -VOTER MODEL WITH ZEALOTS

We consider a population of N voters that can support one of two parties, either A or B, and therefore be in two states. Supporters of party A are in state $+1$, and those supporting party B are in state -1 . Among the voters, a fixed number of them are “inflexible zealots” while the others are “susceptibles”. Here, zealots are individuals that never change opinion: they permanently support either party A (A-zealots) or party B (B-zealots). Susceptible voters can change their opinion under the pressure of a group of neighbors. The population thus consists of a number Z_+ of A-zealots (pinned in state $+1$) and Z_- of B-zealots (pinned in state -1), and a total of $S = N - Z_+ - Z_-$ susceptibles agents, of which n are A-susceptibles (non-zealot voters in state $+1$) and $S - n$ are B-susceptibles (non-zealot voters in state -1). The fraction, or density, of susceptibles in the entire population remains constant and is given by $s = S/N$. For simplicity we assume that all agents have the same persuasion strength.

At each time step, a susceptible voter consults a group of q neighbors (with $q > 1$) and, if there is consensus in the group, the voter is persuaded to adopt the group’s state with rate 1 [14]. The dynamics is a generalization of the nonlinear q VM [14] with a finite density of zealots [10], and consists of the following steps:

1. Pick a random voter. If this voter is a zealot nothing happens.
2. If the picked voter is a susceptible, then pick a group of q neighbors (for the sake of simplicity repetition is allowed, as in Refs. [14, 20]). If all q neighbors are in the same state, the selected voter also adopts that state. Nothing happens in the update if there is no consensus among the q neighbors [21], or if the voter and its q neighbors are already in the same state.
3. Repeat the above steps *ad infinitum* or until consensus is reached.

The case $q = 1$ corresponds to the classical (linear) voter model [1, 8–10], and we therefore focus on $q \geq 2$.

For the sake of simplicity, we investigate this model on a complete graph (well-mixed population of size N). The state of the population is characterized by the probability $P(n, t)$ that the number of A-susceptibles at time t is n . This probability obeys the master equation [22]

$$\begin{aligned} \frac{dP_n(t)}{dt} &= T_{n-1}^+ P_{n-1}(t) + T_{n+1}^- P_{n+1}(t) \\ &\quad - (T_n^+ + T_n^-) P_n(t). \end{aligned} \quad (1)$$

The first line accounts for processes in which the number of A-susceptibles after the event equals n , while the second term accounts for the complementary loss processes

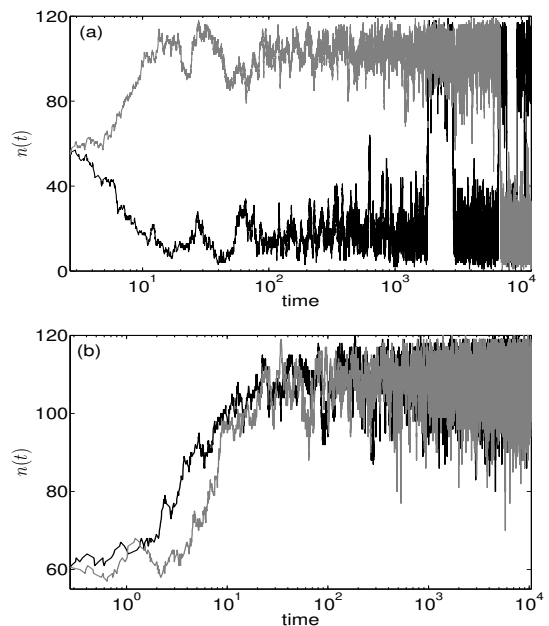


FIG. 1: Number $n(t)$ of A-susceptibles vs. time in two sample realizations (black and gray) at low zealotry, $(Z_+ + Z_-)/2N < z_c$, with initial condition $n(0) = S/2$, see text. Here, $q = 2$, $N = 200$ and $S = 120$. (a) Symmetric zealotry with $Z_+ = Z_- = 40$, $z_c = 0.25$: $n(t)$ continuously fluctuates and suddenly switches from $n \approx S$ to $n \approx 0$ and vice-versa. (b) Asymmetric zealotry with $Z_+ = 43$ and $Z_- = 37$, $z_c = 0.2022$: After a transient, $n(t)$ fluctuates around a value corresponding to a majority of A-susceptibles, see text.

where $n \rightarrow n \pm 1$. Here T_n^\pm represent the rates at which transitions occur and are given by

$$T_n^+ = \left(\frac{S-n}{N} \right) \left(\frac{n+Z_+}{N-1} \right)^q; \quad T_n^- = \frac{n}{N} \left(\frac{S+Z_- - n}{N-1} \right)^q \quad (2)$$

When there are zealots of both types $T_{n=S}^+ = T_{n=0}^- = 0$ and the system has reflective boundaries at $n = 0$ and $n = S$. When there are only A-zealots, $Z_- = 0$ and $Z_+ = N\zeta > 0$, with ζ being the density of A-zealots, then $n = S = N(1 - \zeta)$ is an absorbing boundary with $T_{n=S}^\pm = 0$, while $n = 0$ is reflective. The birth-and-death process (1) is here simulated with the Gillespie algorithm [23] upon rescaling time in Eq. (1) as $t \rightarrow t/N$.

A quantity of particular interest is the magnetization $m = [n + Z_+ - (S - n) - Z_-]/N = [2n - S + Z_+ - Z_-]/N$ that gives the population’s average opinion or, equivalently here, the opinion of a random voter [10]. We have $m = m_{\max} = (S + Z_+ - Z_-)/N$ when all susceptibles are state $+1$ (all A-susceptibles) and $m = m_{\min} = (-S + Z_+ - Z_-)/N$ when all susceptibles are in state -1 (all B-susceptibles), with $m_{\min} \leq m \leq m_{\max}$.

To gain an intuitive understanding of the q VM dynamics, it is useful to consider the evolution of $n(t)$ in typical sample realizations, as those in Fig. 1 where we illustrate the dynamics at low zealotry. In Fig. 1 we notice two distinct regimes and different time-scales. In the case of

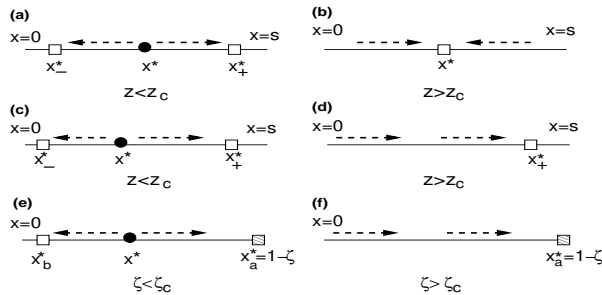


FIG. 2: Schematic of the mean field dynamics when $z_+ = z_- = z$ and $x^* = s/2$ (a,b); when $z_{\pm} = (1 \pm \delta)z > 0$ with $0 < \delta < 1$ (c,d); and $z_+ = \zeta > 0$ with $z_- = 0$ (e,f). (\square) and (\bullet) indicate stable and unstable fixed points, respectively. Panels in the left column correspond to low zealotry $z < z_c$ (a,c) and $\zeta < \zeta_c$ (e); those in the right column correspond to high zealotry $z > z_c$ (b,d) and $\zeta > \zeta_c$ (f), see text.

symmetric low zealotry ($Z_+ = Z_-$), the number of susceptibles first approaches either the state $n \approx 0$ (all B-susceptibles) or $n \approx S$ (all A-susceptibles). After a characteristic time (see Sec. V.A), all susceptibles suddenly start switching from one state to the other, see Fig. 1 (a). A similar feature has been observed in the Sznajd model ($q = 2$) with anticonformity [17]. When $Z_+ > Z_- > 0$, the majority of susceptibles become A-supporters after a typical time (see Sec. V.B). The fluctuations in the number of A-susceptibles then grow endlessly, see Fig. 1 (b). An important aspect of this work is to analyze how demographic fluctuations arising in finite populations alter the mean field predictions. In Section V the phenomena illustrated by Fig. 1 are studied in large-but-finite populations, and we show that these phenomena are beyond the reach of the next section's mean field analysis.

III. MEAN FIELD DESCRIPTION

For further reference, it is useful to consider the mean field (MF) limit of an infinitely large population, $N \rightarrow \infty$. In such a setting, demographic fluctuations are negligible and the rates (2) can be written in terms of the density $x = n/N$ of A-susceptibles, and the densities $z_{\pm} = Z_{\pm}/N$ of zealots of each type: $T_n^+ \rightarrow T^+(x) = (s-x)(x+z_+)^q$ and $T_n^- \rightarrow T^-(x) = x(s+z_- - x)^q$. The MF dynamics is described by the rate equation obtained by averaging n/N from Eq. (1) (and rescaling time as $Nt \rightarrow t$) [22]:

$$\dot{x} = T^+(x) - T^-(x) = (s-x)(x+z_+)^q - x(s-x+z_-)^q, \quad (3)$$

where the dot denotes the time derivative and $s = S/N$.

In the absence of zealotry ($z_{\pm} = 0$, $s = 1$), Eq. (3) has two stable absorbing fixed points, $x = 0$ (all B-supporters) and $x = 1$ (all A-supporters) corresponding to consensus with either A or B party, separated by an unstable fixed point $x = 1/2$ (mixture of A- and B-voters) [14]. It is worth noting that the dynamics of the

q VM without zealots ceases when a consensus is reached and this happens in a finite time when the population size is finite [14–18]. However, in the presence of zealots supporting both parties, the population composition endlessly fluctuates [9, 10], see, *e.g.*, Fig. 1.

In the presence of zealotry, the interior fixed points of Eq. (3) satisfy $T^+(x) = T^-(x)$, which leads to

$$\left(\frac{s-x}{x}\right) \left(\frac{x+z_+}{s-x+z_-}\right)^q = 1. \quad (4)$$

Depending on the values of z_{\pm} and q , this equation has either three physical roots, or a single physical solution.

A. The symmetric case $z_+ = z_- = z$

When the density of zealots of both types is identical, $z_+ = z_- = z$ and $s = 1 - 2z$ with $0 < z < 1/2$, Eq. (3) becomes

$$\dot{x} = (1 - 2z - x)(x+z)^q - x(1 - z - x)^q,$$

that is characterized by a fixed point $x^* = s/2$. When z is sufficiently low, Eq. (3) has two further fixed points: x_+^* and $x_-^* = s - x_+^*$. The analysis for arbitrary $q > 1$ is unwieldy, but insight can be gained by focusing on $q = 2$ and $q = 3$, for which

$$x_{\pm}^* = \begin{cases} \frac{1}{2}(s \pm \sqrt{1-4z}) & (q = 2) \\ \frac{1}{2}\left(s \pm \sqrt{\frac{1-3z}{1+z}}\right) & (q = 3). \end{cases}$$

We readily verify that x_{\pm}^* are both stable when $z < z_c(q)$, with $z_c(2) = 1/4$ and $z_c(3) = 1/3$. When $z > z_c(q)$, the fixed points x_{\pm}^* are unphysical and $x^* = s/2$ is stable. This picture holds for arbitrary finite value of $q > 1$: x_{\pm}^* are stable and the MF dynamics is characterized by bistability below a critical value $z_c(q)$, while $x^* = s/2$ is unstable when $z < z_c$ and stable when $z \geq z_c$, see Fig. 2(a,b). By determining when Eq. (4) has three physical roots, we have found the critical zealotry density

$$z_c(q) = \begin{cases} 1/4 & (q = 2) \\ 1/3 & (q = 3) \\ 3/8 & (q = 4) \\ 2/5 & (q = 5), \end{cases} \quad (5)$$

while $z_c(1) = 0$ since in the linear VM Eq. (3) has always one single stable fixed point [10]. Hence, the value of z_c increases with q , while the values of x_+^* and x_-^* get closer to the values 0 (all B-susceptibles) and s (all A-susceptibles) as q increases with z kept fixed.

In this MF picture, the population's average opinion given by the magnetization $m(t) = 2x(t) - s$ undergoes a supercritical pitchfork bifurcation at $z = z_c$ [24]: At $t \rightarrow \infty$, the critical value z_c separates an ordered phase ($z < z_c$), where a majority of susceptibles supports one party, from a disordered phase ($z > z_c$) in which each party is supported by half of the susceptibles, see Fig. 2

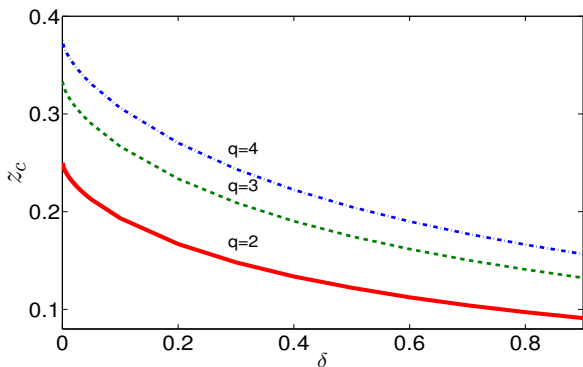


FIG. 3: (*Color Online*) Critical value of z_c as a function $\delta = (z_+ - z_-)/2z$ for $q = 2$ (solid), $q = 3$ (dashed), and $q = 4$ (dash-dotted) in the case of asymmetric zealotry. There is bistability where $z = (z_+ - z_-)/(2\delta) < z_c$, see text.

(a,b). The stationary MF magnetization thus depends on the initial condition: when $z < z_c$, $m(\infty) = m^* = 2x_+^* - s$ if $m(0) > 0$ and $m(\infty) = -m^*$ if $m(0) < 0$, while the magnetization vanishes when $z \geq z_c$ (or if $m(0) = 0$). Using Eqs. (4) and (5), it can be directly checked that just below the critical zealotry density, i.e. for $z \lesssim z_c$, the stationary magnetization is characterized by the scaling relationship $m(\infty) \propto m^* \sim \sqrt{z_c - z}$.

B. The asymmetric case $z_{\pm} = (1 \pm \delta)z$

When the number of A-zealots exceeds that of B-zealots, with $z_+ > z_- > 0$, it is convenient to use the parametrization

$$z_{\pm} = (1 \pm \delta)z, \quad (6)$$

where $\delta = (z_+ - z_-)/2z$ quantifies the zealotry asymmetry. With Eq. (6), we still have $s = 1 - 2z$ with $0 < z < 1/2$ and Eq. (3) becomes

$$\dot{x} = (1 - 2z - x)[x + (1 + \delta)z]^q - x[1 - (1 + \delta)z - x]^q.$$

This rate equation is also characterized by bistability at low zealotry, with two stable fixed points x_{\pm}^* separated by an unstable fixed point x^* , and by the sole stable fixed point x_+^* at higher zealotry, see Fig. 2(c,d). By determining when Eq. (3) has three physical fixed points, we have determined the critical density of zealotry $z_c(q, \delta)$, see Fig. 3: At fixed q and δ , the fixed points x_{\pm}^* are stable when $z < z_c$ while only x_+^* is stable when $z \geq z_c$. We have found that z_c decreases with δ (at fixed q) and increases with q (at fixed δ).

In this MF picture, the opinion of a random individual is given by the magnetization $m(t) = 2(x + \delta z) - s$. The critical zealotry density z_c separates a bistable phase ($z < z_c$) from a phase where most susceptibles support the party having more zealots, see Fig. 2 (c,d). Hence, the stationary MF magnetization at low zealotry ($z < z_c$)

depends on the initial condition and is $m(\infty) = m_+^* = 2(x_+^* + \delta z) - s$ if $m(0) > 2(x_+^* + \delta z) - s$ and $m(\infty) = m_-^* = 2(x_-^* + \delta z) - s$ if $m(0) < 2(x_+^* + \delta z) - s$. When $z > z_c$ the stationary MF magnetization is $m(\infty) = m_+^*$.

C. The absorbing case $z_+ = \zeta, z_- = 0$

When there are only A-zealots, $z_+ = \zeta > 0$ and $z_- = 0$, Eq. (3) becomes

$$\dot{x} = (1 - \zeta - x) [(x + \zeta)^q - x(1 - \zeta - x)^{q-1}],$$

and has an absorbing fixed point $x_a^* = 1 - \zeta$. Below a critical zealotry density $\zeta_c(q)$, this rate equation admits two other fixed points: x_b^* , that is stable, and x^* that is unstable and separates x_a^* and x_b^* , see Fig. 2(e,f). When $\zeta > \zeta_c(q)$, the absorbing state $x_a^* = 1 - \zeta$ is the only fixed point. For $q = 2$ and $q = 3$, we explicitly find

$$x_b^* = \begin{cases} \frac{1}{4} (1 - 3\zeta - \sqrt{1 - (6 - \zeta)\zeta}) & (q = 2) \\ \frac{1 - 2\zeta(1 + \zeta) - \sqrt{1 - 4\zeta}}{2(2 + \zeta)} & (q = 3) \end{cases} \quad (7)$$

and

$$x^* = \begin{cases} \frac{1}{4} (1 - 3\zeta + \sqrt{1 - (6 - \zeta)\zeta}) & (q = 2) \\ \frac{1 - 2\zeta(1 + \zeta) + \sqrt{1 - 4\zeta}}{2(2 + \zeta)} & (q = 3) \end{cases} \quad (8)$$

From these expressions, and more generally by determining when Eq. (4) has three physical roots, we have found the critical zealotry density in the absorbing case:

$$\zeta_c(q) = \begin{cases} 3 - 2\sqrt{2} & (q = 2) \\ 1/4 & (q = 3) \\ 0.295 & (q = 4) \\ 0.326 & (q = 5) \end{cases} \quad (9)$$

We thus distinguish two regimes:

(i) When $\zeta > \zeta_c(q)$, as well as when $\zeta = \zeta_c$ and $x_0 > x^*$, the absorbing state is rapidly reached.

(ii) When $\zeta < \zeta_c(q)$ both $x_{a,b}^*$ are stable and the dynamics crucially depends on the initial density x_0 of A-susceptibles: If $x_0 > x^*$, the final state is the consensus with party A; whereas the steady state consists of a vast majority of B-party voters when $x_0 < x^*$. In Section VI, we show that random fluctuations drastically alter this picture: In a finite population, x_b^* is a metastable state when $\zeta < \zeta_c(q)$ and $x_0 < x^*$, and we shall see that the A-consensus is reached after a very long transient that scales exponentially with the population size.

IV. STATIONARY PROBABILITY DISTRIBUTION

In this section, we compute the stationary probability distribution (SPD) of the q VSM with zealotry when there

is no absorbing state, and show that its shape generally differs from the Gaussian-like distribution obtained in the linear VM with zealots [10].

The SPD $P_n^* = \lim_{t \rightarrow \infty} P_n(t)$ obeys the following stationary master equation, obtained from Eq. (1):

$$T_{n-1}^+ P_{n-1}^* + T_{n+1}^- P_{n+1}^* - (T_n^+ + T_n^-) P_n^* = 0.$$

The exact SPD is uniquely obtained by iterating the detailed balance relation $T_{n-1}^+ P_{n-1}^* = T_n^- P_n^*$ [22], yielding

$$\begin{aligned} P_n^* &= P_0^* \prod_{j=0}^{n-1} (T_j^+ / T_{j+1}^-) \\ &= P_0^* \prod_{j=0}^{n-1} \left(\frac{S-j}{j+1} \right) \left(\frac{j+Z_+}{S+Z_- - j - 1} \right)^q, \end{aligned} \quad (10)$$

where the normalization $\sum_{n=0}^S P_n^* = 1$ gives $P_0^* = 1 / [1 + \sum_{k=1}^S \prod_{j=0}^{k-1} (T_j^+ / T_{j+1}^-)]$ and $P_S^* = 1 - P_0^* - \sum_{k=1}^{S-1} P_k^*$.

Since $n = N[(m+s)/2 - \delta z]$, the stationary magnetization distribution Q_m^* has the same shape as P_n^* , with

$$\begin{aligned} Q_m^* &= P_{N[(m+s)/2 - \delta z]}^* \\ &= P_0^* \prod_{j=0}^{N[(m+s)/2 - \delta z] - 1} \left(\frac{S-j}{j+1} \right) \left(\frac{j+Z_+}{S+Z_- - j - 1} \right)^q. \end{aligned} \quad (11)$$

In large populations, a useful approximation of (10) is obtained by writing $P_n^* = P_0^* \exp\left(\sum_{j=0}^{n-1} \Psi_j\right)$ with $\Psi_j = \ln(T_j^+ / T_{j+1}^-)$, and by using Euler-MacLaurin formula $\sum_{j=0}^{n-1} \Psi_j = \int_0^{n-1} \Psi_j dj + (\Psi_0 + \Psi_{n-1})/2$, where we have neglected higher order terms [26].

When $N \gg 1$, it is useful to work in the continuum limit with the rates $T_n^\pm \rightarrow T^\pm(x)$, as in Sec. III. By introducing

$$\Psi(x) = \ln[T^+(x)/T^-(x)], \quad (12)$$

we have $\sum_{j=0}^{n-1} \Psi_j \simeq N \int_0^x \Psi(x) dx$ to leading order in N . Hence, the leading contribution to the SPD when $N \gg 1$ is

$$P_n^* \sim P_0^* \exp\left(N \int_0^x \Psi(y) dy\right) = P^*(x). \quad (13)$$

The local extrema of $P^*(x)$ satisfy $\Psi(x) = 0$, see (12), and thus coincide with the fixed points of Eq. (3). As a consequence, in large populations P_n^* is either characterized by a single peak at $n^* = Nx^*$ when $z > z_c$, or has two peaks at the metastable states $n_\pm^* = Nx_\pm^*$ when $z < z_c$. In this case, there is bistability and the amplitudes of the peaks at n_\pm^* are in the ratio ($N \gg 1$)

$$\frac{P_{n_\pm^*}^*}{P_{n_\mp^*}^*} \sim e^{N \int_{x_\mp^*}^{x_\pm^*} \Psi(y) dy}. \quad (14)$$

The integrals in Eqs. (13) and (14) can be computed, but their expressions are unenlightening. Here, we infer the properties of $P_n^* \sim P^*(x)$ and Q_m^* from those of $\Psi(x)$.

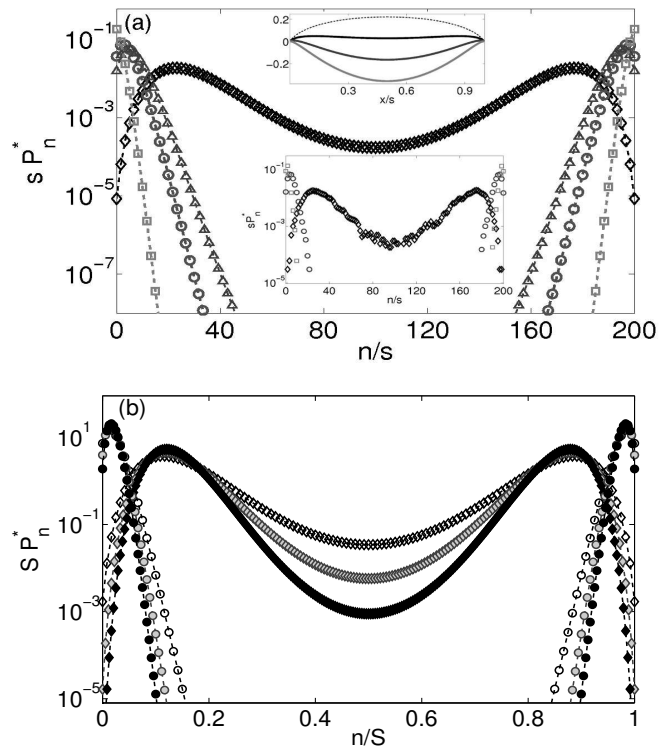


FIG. 4: Rescaled SPD at low zealotry with $z_+ = z_- = z < z_c$ in semi-log scale. (a) sP_n^* vs. n/s from Eq. (10) for different values of q and z , with $N = 200$. Here, $q = 2, z = 0.2$ (\diamond); $q = 3, z = 0.22$ (Δ); $q = 3, z = 0.2$ (\circ) and $q = 4, z = 0.2$ (\square). Lower inset: Similar; sP_n^* vs. n/s from stochastic simulations. Upper inset: $\int_0^x \Psi(y) dy$ vs. x/s for $z = 0.2$ and, from top to bottom, $q = 1$ (dashed), $q = 2$ (black), $q = 3$ (gray) and $q = 4$ (light gray). (b) SP_n^* vs. n/S from Eq. (10) for $q = 2$ (diamonds) and $q = 3$ (circles), and for different values of the population size N at low zealotry. Here, $z = 0.2$ and $N = 200$ (open symbols), $N = 300$ (gray-filled symbols) and $N = 400$ (black-filled symbols). Not shown in panels (a) and (b) is the range where $P_n^* \lesssim 10^{-8}$ (where $P_n^* \lesssim 10^{-5}$ in the lower inset).

A. Stationary probability distribution in the symmetric case

In the symmetric case, $z_+ = z_- = z$, Eq. (12) becomes

$$\Psi(x) = \ln \left[\left(\frac{1 - (x + 2z)}{x} \right) \left(\frac{x + z}{1 - (x + z)} \right)^q \right]$$

and has the symmetry $\Psi(x) = -\Psi(s-x)$. We distinguish the cases of low and high zealotry density:

(i) When $z < z_c(q)$, the fixed points x^* and x_\pm^* of Eq. (3) are also the roots of $\Psi(x)$. Hence, when $N \gg 1$, $P_n^* = P_{S-n}^* \sim P^*(x) \propto e^{N \int_0^x \Psi(y) dy}$ is a symmetric bimodal SPD characterized by two peaks at $n = n_\pm^*$. As a consequence, $Q_m^* = Q_{-m}^*$ is an even function.

In Figure 4 (a), we show the exact SPD for $q = 2 - 4$ characterized by two peaks of same intensity at $n = n_\pm^*$ and a local minimum at $n^* = S/2$. We remark that when

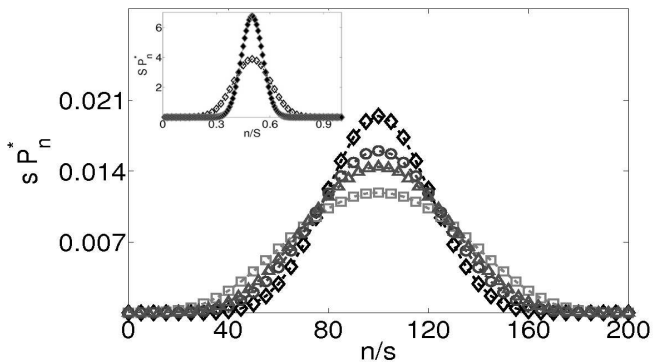


FIG. 5: sP_n^* vs. n/s for $q = 2 - 4$ at high zealotry $z > z_c$. Here, $N = 200$ and $(q, z) = (2, 0.4)$ (\diamond), $(3, 0.4)$ (\circ), $(3, 0.375)$ (Δ), $(4, 0.4)$ (\square). The SPDs have a single peak at $n/s = N/2$ and width broadens when q and $1/z$ are increased at fixed N . Inset: sP_n^* vs. n/S for $q = 2$ and different population values of N . Here, $N = 200$ (\diamond) and $N = 600$ (\blacklozenge).

q is increased, the SPD vanishes dramatically away from the peaks. In fact, since $\int_0^x \Psi(y) dy$ is close to zero or negative on $x_-^* \ll x \ll x_+^*$, see Fig. 4 (a, upper inset), $P_{n_-^* \ll n \ll n_+^*}^*$ vanishes exponentially with N and when q is increased. Fig. 4(a) shows that the SPD steepens and its peaks are more pronounced when q and $1/z$ are increased and N is kept fixed. We have also obtained the (quasi-)SPD from stochastic simulations, see Fig. 4 (a, lower inset), by averaging over 25,000 realizations after 40,000 simulation steps. While unavoidably more noisy, the simulation results reproduce the predictions of Eq. (10). Fig. 4(b) shows how sP_n^* scales with $n/S = x/s$ for different population sizes, and notice that the main influence of raising N is to concentrate the probability density sP_n^* around the peaks whose location are essentially unaffected by N (when $N \gg 1$). In Fig. 4, we also notice that the symmetric peaks are clearly identifiable when $q = 2$ and $q = 3$, but almost coincide with $n = 0$ and $n = S$ for $q = 4$. This is because x_{\pm}^* approach the values $x = 0, s$ when q is increased.

(ii) When $z \geq z_c$, the only physical root of $\Psi(x)$ is $x^* = s/2$, as in the classical voter model [10]. Hence, $P_n^* = P_{S-n}^* \sim P^*(x) \propto e^{N \int_0^x \Psi(y) dy}$ has a single maximum at $x = s/2$ when $N \gg 1$. The resulting symmetric Gaussian-like distribution centered at $n^* = S/2$ when $N \gg 1$, see Fig. 5, is very similar to the SPD obtained in the classical voter model with zealots [10]. Fig. 5(inset) illustrates that the probability density steepens around $s/2$ when the population size is increased.

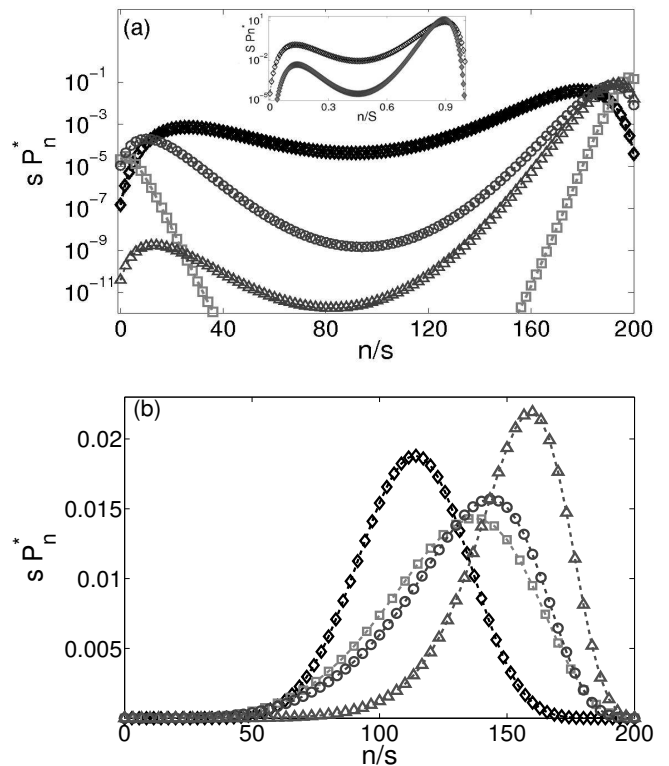


FIG. 6: Rescaled SPD under asymmetric zealotry $Z_{\pm} = N(1 \pm \delta)z$. (a) sP_n^* vs. n/s from Eq. (10) at low zealotry ($z < z_c$). Here, $N = 200$ and $(q, Z_+, Z_-) = (2, 41, 39)$ (\diamond), $(3, 51, 49)$ (\circ), $(3, 53, 47)$ (Δ), $(4, 51, 49)$ (\square). For $q = 4$, the range where $P_n^* \lesssim 10^{-12}$ is not shown. Inset: sP_n^* vs. n/S for $q = 2$ and $(N, Z_+, Z_-) = (200, 41, 39)$ (open \diamond), $(400, 82, 78)$ (gray-filled symbols). (b) Left-skewed rescaled SPD at high zealotry, with a single peak at n_+^* . Here, $N = 200$ and $(q, Z_+, Z_-) = (2, 67, 63)$ (\diamond), $(3, 72, 68)$ (\circ), $(3, 74, 66)$ (Δ), $(4, 82, 78)$ (\square), see text.

B. Stationary probability distribution in the asymmetric case

In the asymmetric case, with zealot densities $z_{\pm} = (1 \pm \delta)z$ and $\delta > 0$, Eq. (12) is

$$\Psi(x) = \ln \left[\left(\frac{1 - (x + 2z)}{x} \right) \left(\frac{x + z(1 + \delta)}{1 - z(1 + \delta) - x} \right)^q \right]$$

and has either three or one physical roots:

(i) At fixed q and δ , when $z < z_c(q, \delta)$, the fixed points x^* and x_{\pm}^* of Eq. (3) are the physical roots of $\Psi(x)$. Since $P_n^* \sim P^*(x) \propto e^{N \int_0^x \Psi(y) dy}$ when $N \gg 1$, the SPD is again a bimodal distribution peaked at n_{\pm}^* . However, x_+^* has a greater basin of attraction than x_-^* and $\int_{x_+^*}^{x_-^*} \Psi(y) dy > 0$. As a consequence, the SPD is asymmetric, with the peak at n_+^* being much stronger than the one at n_-^* . The ratio of the peaks is given by (14), which shows that the asymmetry of P_n^* grows exponentially with N and increases with q , see Fig. 6(a). While

an asymmetry in the zealotry in the linear VM does not significantly affect the form of the SPD [10], we here find that in the q VM even a small bias in the zealotry drastically changes the shape of the SPD and leads to marked dominance of the party with more zealots.

In Fig. 6 (a), we report the exact SPD for $q = 2-4$ and illustrate its asymmetric bimodal nature, with marked peaks of different intensities at n_{\pm}^* . We notice that the asymmetry in the peaks intensity, given by (14), is stronger when we increase q and $Z_+ - Z_- \propto \delta z$. As in the symmetric case, the SPD decays dramatically away from the peaks and $P_{n_{\pm}^*}^* \ll n \ll n_{\pm}^*$ vanishes with $N \gg 1$ and when q is increased. In Fig. 6 (a, inset) we show that the SPD remains bimodal when the population size is increased (with $N \gg 1$), and the main influence of raising N is to concentrate the probability density near its peak at $x_{\pm}^* = n_{\pm}^*/N$.

(ii) At fixed q and δ , when $z > z_c$, the only real root of $\Psi(x)$ is $x = x_+^*$. This lies closer to $x = s$ than to $x = 0$, and hence $\int_0^x \Psi(y) dy$ is an asymmetric function with a single maximum at $x = x_+^*$. Therefore, in large populations P_n^* is an asymmetric left-skewed SPD with a single peak at $n = n_+^*$, as shown in Fig. 5(b) where we see that the SPD broadens when q is increased and that it steepens when $Z_+ - Z_- \propto \delta z$ is increased. As above, the probability density steepens around x_+^* when N is increased.

V. FLUCTUATION-DRIVEN DYNAMICS AT LOW ZEALOTRY

We now study how a small non-zero density of zealots of both parties ($0 < z < z_c$) affects the q VM long-time dynamics. We show that, after a typically long transient, all susceptible voters switch allegiance from the state $n = 0$ (all B-susceptibles) to state $n = S$ (all A-susceptibles) in a typical switching time. In the symmetric case, there is “swing-state dynamics” with all susceptibles endlessly swinging allegiance. In the asymmetric case where party A has more zealots than party B, the dynamics is characterized by various time-scales and by growing fluctuations around the metastable state n_{\pm}^* . Below, we show that the long-time q VM dynamics is driven by fluctuations and characterized by a mean switching time that scales (approximately) exponentially with the system size N in large-but-finite populations.

A. Swing-state dynamics and switching time in the case of symmetric zealotry

As illustrated in Fig. 1(a), the long-time dynamics in the symmetric case is characterized by the continuous swinging from states $n \approx 0$ to $n \approx S$ and vice versa. When $Z_+ = Z_-$, all susceptibles thus continuously switch allegiance in the long run. In that regime,

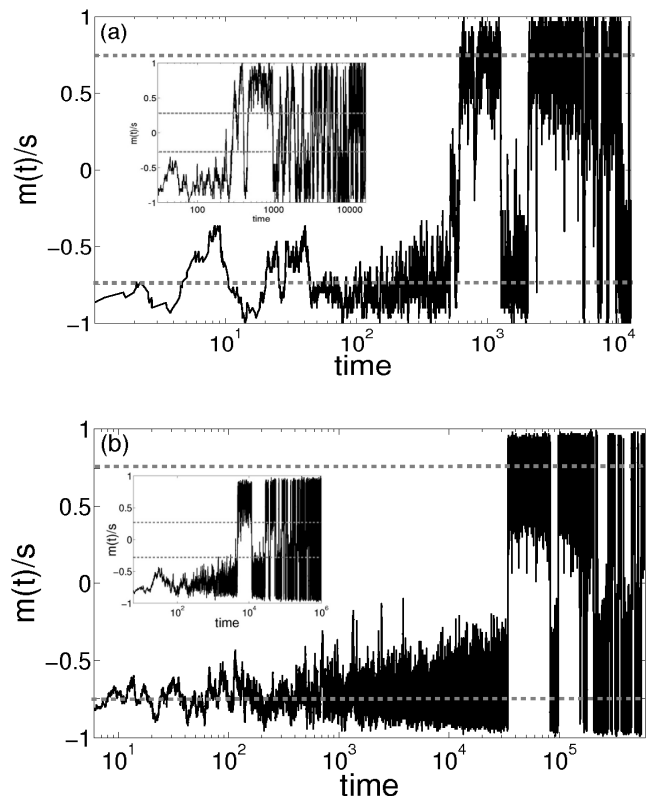


FIG. 7: Typical evolution of the rescaled magnetization for different values of q and N with initial condition $m(0) = -s$ (all B-susceptibles) on a semi-log scale: (a) Single realization of $m(t)/s$ for $q = 2, z = z_+ = z_- = 0.2 < z_c$ and population size $N = 100$. At time $t \approx 625$, $m = s$ and starts swinging back and forth the values $m = \pm s$. Here, the MF predicts $m^* \approx 0.745$ and $\pm m^*$ are shown as dashed lines. Inset: $m(t)/s$ vs. time for $q = 3, z = 0.3 < z_c$ and $N = 100$. The system starts swinging between $m = \pm s$ at $t \approx 640$. Here, $\pm m^* \approx \pm 0.277$ (dashed). (b) $m(t)/s$ vs. time for the same parameters as in (a) but with $N = 300$. The system’s magnetization switches to $m = s$ only at $t \approx 2 \cdot 10^5$. Inset: $m(t)/s$ vs. time for $q = 3, z = 0.3$ and $N = 400$. The magnetization switches to $m = s$ at $t \approx 3 \cdot 10^5$. The difference in the switching times in (a) and (b) results from the exponential scaling of the mean switching time on N , see text.

the magnetization $m(t) = (2n(t) - S)/N$ is thus characterized by abrupt jumps from $m \approx \pm s$ to $m \approx \mp s$, see Fig. 7, while the stationary ensemble-averaged magnetization $\langle m(\infty) \rangle = \sum_{m=-s}^s m Q_m^* = 0$, since Q_m^* is even and each agent is as likely to be in one or the opposite state. A similar phenomenon has been found in the Sznaid model ($q = 2$) with anticonformity [17].

This swing-state phenomenon is not captured by the mean field description of Sec. III and is here characterized by the mean time τ_0^S to switch for the first time from state $n = 0$ to $n = S$. The scaling of τ_0^S on N allows us to rationalize the data of Fig. 7 where the switching time is found to dramatically increase with the population size.

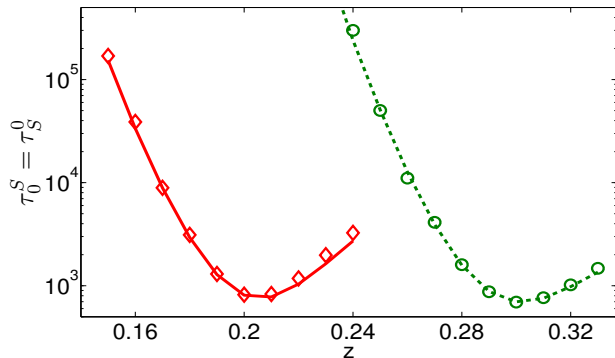


FIG. 8: (*Color Online*) Mean switching time τ_0^S vs. z in the symmetric case $z_+ = z_- = z < z_c$ for $q = 2$ (\diamond , solid), $q = 3$ (\circ , dashed) and $N = 100$. Symbols are results of stochastic simulations and lines are the predictions of (17), see text.

Clearly, the symmetry implies that the mean switching, or swinging, time τ_0^S is identical to the mean time τ_S^0 to switch from $n = S$ to $n = 0$.

Finding the mean switching time can be formulated as a first-passage time problem and, when $N \gg 1$, τ_0^S can be computed using the framework of the backward Fokker-Planck equation (bFPE) [22]. In this context, the model's bFPE infinitesimal generator is

$$\mathcal{G}_b(x) = [T^+(x) - T^-(x)]\partial_x + \frac{[T^+(x) + T^-(x)]}{2N}\partial_x^2. \quad (15)$$

The mean time $\tau^S(x_0)$ to be absorbed at $x = s$ (all A-susceptibles) starting from the initial state $x = x_0$, with a reflective boundary at $x = 0$ (all B-susceptibles) obeys

$$\mathcal{G}_b(x_0) \tau^S(x_0) = -1, \quad (16)$$

with $(d/dx)\tau^S(0) = 0$ and $\tau^S(s) = 0$ (reflective/absorbing boundaries) [22, 25]. To obtain the mean switching time τ_0^S we solve Eq. (16) with $x_0 = 0$ using standard methods [22], and obtain

$$\tau_0^S = 2N \int_0^s dy e^{-N\phi(y)} \int_0^y \frac{e^{N\phi(v)} dv}{T^+(v) + T^-(v)}, \quad (17)$$

where $\phi(v) = -2 \int_0^v du \left\{ \frac{T^-(u) - T^+(u)}{T^-(u) + T^+(u)} \right\}$. As with other fluctuation-driven phenomena associated with metastable states, see *e.g.* [25, 27–30] and below, this result predicts that the mean switching time τ_0^S grows (approximately) exponentially with the population size N . This explains the difference of various orders of magnitude in the switching time observed in the panels (a) and (b) of Fig. 7.

The predictions of (17) are reported in Fig. 8 for various values of $z < z_c$. These are in good agreement with the results of numerical simulations (averaged over 1000 samples, each run for 10^6 simulation steps). When z is lowered well below z_c , the peaks of the SPD approach

$n = 0$ and $n = S$. In this case, τ_0^S increases and switching allegiance takes very long. At fixed $z < z_c$, we find that τ_0^S increases with q . Interestingly, we also find that τ_0^S can exhibit a non-monotonic dependence on z just below z_c when q is kept fixed, as shown in Fig. 8.

B. Time-scale separation and growing fluctuations in the asymmetric case

In the asymmetric case $0 < z_- < z_+$, the party A has more zealot supporters than party B. In this situation, when $z < z_c$ the SPD has a marked peak near $n = S$, see Fig. 6(a). As shown in Fig. 1(b), the long time dynamics is characterized by a large majority of susceptibles becoming A supporters independently of the initial state. The magnetization $m(t) = 2\delta z + [2n(t) - S]/N$ thus fluctuates around its MF value m_+^* before reaching $m = m_{\max} = s + 2\delta z$ when all susceptibles are supporters of party A, see Fig. 9(a). The population composition then endlessly fluctuates, with a majority of susceptibles supporting party A. In this case, with Eq. (11), the stationary ensemble-averaged magnetization $\langle m(\infty) \rangle = \sum_{m=m_{\min}}^{m_{\max}} m Q_m^*$ is positive.

The q VM dynamics is thus characterized by various regimes not captured by the mean field description. For concreteness, we consider that the initial density of A-susceptibles is $x_0 < x_-^*$, as in Fig. 9, and distinguish four time scales:

(i) After a mean time of order τ_{r_1} , the system quickly relaxes toward the metastable state n_-^* where a random voter has the MF opinion m_-^* , see Fig. 9(a).

(ii) After a mean time τ_-^+ , almost all realizations suddenly approach the metastable state n_+^* where $m(t) \approx m_+^*$, see Figs. 1(a) and 9(b). The mean transition time τ_-^+ , as well as the average relaxation times, can be estimated using Kramers' classical escape rate theory [27]. The latter gives the mean transition time τ_K between the two local minima of the double-well potential $U(x)$ in which an overdamped Brownian particle is moving subject to a zero-mean delta-correlated Gaussian white noise force $\xi(t)$. Here, we consider a potential $U(x)$ such that $dU/dx = T^-(x) - T^+(x)$, and the noise correlations $\langle \xi(t)\xi(t') \rangle = \delta(t-t') [T^+(x_-^*) + T^-(x_-^*)]/N$. The bFPE generator of this Brownian particle is (15) with a constant diffusive term evaluated at x_-^* . Kramer's formula hence gives [25, 27]:

$$\tau_-^+ \simeq \tau_K = 2\pi \tau_{r_1} \tau_{r_2} e^{2N \int_{x_-^*}^{x_+^*} \frac{T^-(y) - T^+(y)}{T^-(x_-^*) + T^+(x_-^*)} dy},$$

where $\tau_{r_1} = 1/\sqrt{U''(x_-^*)}$, and $\tau_{r_2} = 1/\sqrt{|U''(x_+^*)|}$ denotes the mean relaxation time from state $n = n^*$ to $n = n_+^*$.

(iii) The system then fluctuates around n_+^* before reaching the state $n = S$ (all A-susceptibles) where $m = m_{\max}$, see Fig. 9(a) after a mean time τ^S . In the realm of the bFPE, the mean time τ^S for all susceptibles

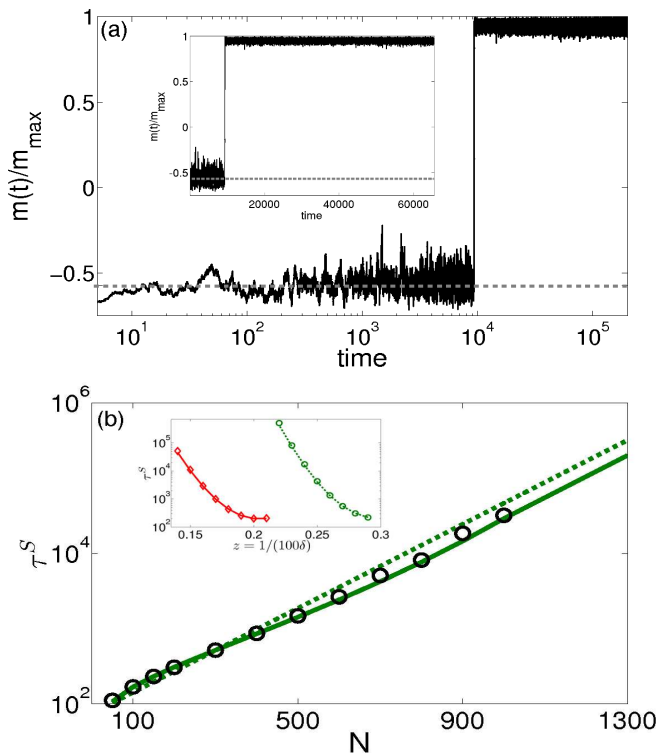


FIG. 9: (Color Online) (a) Typical single realization of $m/m_{\max} = m/(s + 2\delta z)$ in the asymmetric case at low zealotry, with $q = 3$ and $m(0) = m_{\min} = -s + 2\delta z$ (all B-susceptibles). Here, $z = 0.25$, $\delta = 0.12$ and $N = 1000$. After a time $t \approx 15$ the magnetization fluctuates around m_{\min}^* (dashed line); at time $t \approx 6 \cdot 10^4$ it attains $m_{\max} = s + 2\delta z$. In principle, the magnetization can return to m_{\min} (all B-susceptibles) after an enormous time ($\sim 10^{85}$, not shown). Inset: Same, but in linear scale. (b) τ^S as a function of N for $q = 3$, $z = 0.25$ and $\delta = 0.12$. Symbols (\circ) are the results of stochastic simulations. The solid and dashed lines are the predictions of (18) and (19), respectively, showing that τ^S grows approximately exponentially with N , see text. Inset: τ^S vs. $z = (100\delta)^{-1}$ with $N = 100$, and $Z_+ - Z_- = 2$ kept fixed, for $q = 2$ (\diamond , solid) and $q = 3$ (\circ , dashed).

to become A supporters for the first time is

$$\tau^S = 2N \int_{x_0}^s dy e^{-N\phi(y)} \int_0^y \frac{e^{N\phi(v)} dv}{T^+(v) + T^-(v)}. \quad (18)$$

When n_+^* is close to the state $n = S$, the main contribution to τ^S is given by the mean transition time τ_-^+ that is independent of $x_0 < x_-^*$, as in Fig. 9. This is well approximated by Kramer's formula, yielding

$$\tau^S \sim \tau_-^+ \simeq 2\pi \tau_{r_1} \tau_{r_2} e^{2N \int_{x_-^*}^{x_+^*} \frac{T^-(y) - T^+(y)}{T^-(x_-^*) + T^+(x_+^*)} dy}, \quad (19)$$

showing that the mean switching time scales exponentially with the population size.

(iv) The amplitude of the fluctuations around $n \approx S$, where $m(t) \approx m_{\max}$ grows endlessly in time, see

Fig. 1(b), and the system eventually returns to the state $n = 0$ (all B-susceptibles). Yet, this occurs after an enormous amount of time, of order $e^{2N \int_{x_+^*}^{x_-^*} \frac{T^-(y) - T^+(y)}{T^-(x_+^*) + T^+(x_+^*)} dy}$, that is generally not physically observable when $N \gg 1$.

The predictions (18) and its approximation (19) are reported in Fig. 9(b), where they are in good agreement with the results of stochastic simulations. These results confirm that τ^S grows approximately exponentially with N when $N \gg 1$. In Fig. 9(b), we also see that τ^S increases with $1/z$, and with q when z and δ are fixed. As illustrated in Fig. 9(a), contrary to the case of symmetric zealotry, there is no ‘‘swing-state dynamics’’: After a mean time τ^S the population persists near $n \approx S$ where most susceptibles are A supporters and the magnetization is $m \approx m_{\max}$, and there is virtually no switching back to state $n \approx 0$. Hence, a small bias in the zealotry, combined with fluctuations and nonlinearity, can greatly affect the voters' opinion in the q VM.

VI. MEAN CONSENSUS TIME IN THE PRESENCE OF ONE TYPE OF ZEALOTS

When there are only A-zealots, with $z_+ = \zeta$ and $z_- = 0$, an A-party consensus is always reached. Yet, the dynamics leading to the corresponding absorbing state $n = S$ depends non-trivially on the zealotry density and on the initial density x_0 of A-susceptibles.

Here, the fluctuation-driven dynamics is characterized by the mean consensus time (MCT). As illustrated in Fig. 10(a), even for values of ζ and x_0 that are close, the MCT can vary by several order of magnitudes: (i) Below the critical zealotry density ζ_c , the MCT grows exponentially with the population size N when $x_0 < x^*$, see Fig. 10(b); (ii) Otherwise the MCT grows logarithmically with N , see Fig. 10(inset). These phenomena are analyzed as follows:

(i) When $\zeta \leq \zeta_c$ and $x_0 < x^*$, in line with the MF analysis, the density of A-susceptibles first lingers around the metastable state x_b^* until a large fluctuation drives the system towards the absorbing state. This large-fluctuation-driven phenomenon is particularly well captured by the WKB theory [28–30]. The essence of this method consists of studying the quasi-stationary probability distribution (QSPD) π_n obtained by setting $P_n(t) \simeq \pi_n e^{-t/\tau_c}$ for $0 \leq n < S$ and $P_S(t) \simeq 1 - e^{-t/\tau_c}$ into the master equation (1). The MCT is the mean decay time τ_c of the QSPD. Since $(d/dt)P_S \simeq e^{-t/\tau_c}/\tau_c \simeq T_{S-1}^+ \pi_{S-1} e^{-t/\tau_c}$, we indeed find [29, 30]

$$\tau_c = (T_{S-1}^+ \pi_{S-1})^{-1}. \quad (20)$$

The computation of the MCT therefore requires finding the QSPD. This obeys

$$T_{n-1}^+ \pi_{n-1} + T_{n+1}^- \pi_{n+1} - (T_n^+ + T_n^-) \pi_n = 0, \quad (21)$$

obtained from Eq. (1) upon neglecting an exponentially small term π_n/τ_c . In the limit $N \gg 1$, the density $x =$

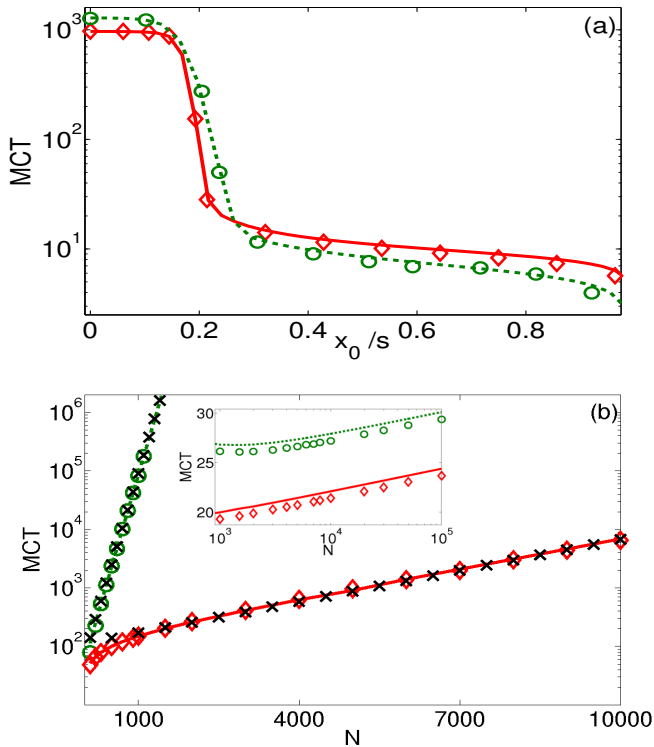


FIG. 10: (*Color Online*) (a) MCT vs. x_0/s for $q = 2, \zeta = 0.17$ and $N = 5000$ (\circ , solid), and $q = 3, \zeta = 0.24$ and $N = 400$ (\circ , dashed). Symbols are from stochastic simulations and lines are the predictions of (26). (b) MCT vs. N for $q = 2, \zeta = 0.17$ (\diamond , solid), and for $q = 3, \zeta = 0.24$ (\circ , dashed). Initially $x_0 = 0.1 < x^*$. Symbols (\diamond) and (\circ) are from simulations (averaged over $10^3 - 10^5$ samples), lines are the predictions of (26) and (\times) are proportional to the WKB results (24)-(25). Inset: MCT vs. N in semi-log scale for $q = 2, \zeta = 0.2$ (\diamond , solid), and for $q = 3, \zeta = 0.26$ and (\circ , dashed).

n/N is treated as a continuous variable and Eq. (20) yields $\tau_c^{-1} = (\pi(s)/N) \left| \frac{d}{dx} T^+(x) \right|_{x=s}$. In the continuum limit, Eq. (21) is solved with the WKB Ansatz

$$\pi(x) \simeq \mathcal{A} e^{-NS(x) - \mathcal{S}_1(x)}, \quad (22)$$

where $\mathcal{S}(x)$ is the action, $\mathcal{S}_1(x)$ is the amplitude, and $\mathcal{A} \sim e^{NS(x_b^*)}$ is a normalization constant [30]. By substituting (22) into (21), to leading order we find [29, 30]

$$\mathcal{S}(x) = - \int^x \Psi(y) dy, \quad (23)$$

where, as in Sec. IV, $\Psi(y) = \ln [T^+(y)/T^-(y)]$.

Hence, when $x_0 < x^*$ and $N \gg 1$, the leading contribution to the MCT is given by the accumulated action $\Delta\mathcal{S}$ over the path joining the metastable state $x = x_b^*$ and the unstable steady state $x = x^*$ [29, 30]:

$$\tau_c \sim e^{N[\mathcal{S}(x^*) - \mathcal{S}(x_b^*)]} = e^{N\Delta\mathcal{S}}. \quad (24)$$

The next-to-leading correction arising from $\mathcal{S}_1(x)$ is given in Refs. [29, 30], but for our purpose Eq. (24) already provides useful information of the MCT. In fact, for $q = 2$ and $q = 3$, the action (23) explicitly reads

$$-\mathcal{S}(x) = \begin{cases} (1 - \zeta) \ln(1 - \zeta - x) + 2\zeta \ln(x + \zeta) \\ + x \ln \left[\frac{(x + \zeta)^2}{x(1 - \zeta - x)} \right] & (q = 2) \\ \zeta \ln x + 2 \ln(1 - \zeta - x) \\ + (x + \zeta) \ln \left[\frac{(x + \zeta)^3}{x(1 - \zeta - x)^2} \right] & (q = 3) \end{cases} \quad (25)$$

With these expressions, and with (7) and (8) for x_b^* and x^* , the leading contribution to the WKB approximation of the MCT is computed explicitly, and the results reported in Fig 10(b) are in excellent agreement with those of stochastic simulations when $N \gg 1$ and confirm that τ_c grows exponentially with N . We can also check that $\Delta\mathcal{S}$ is a decreasing function of ζ , which clearly implies that the MCT grows when ζ is decreased.

(ii) When $\zeta > \zeta_c$, or for any $\zeta > 0$ when the initial density $x_0 > x^*$, the A-party consensus is reached much quicker than in the case (i), typically after a time of order $\mathcal{O}(\ln N)$, see Fig. 10(inset). The backward Fokker-Planck formalism is again suitable to derive this result. In such a framework, the MCT obeys Eq. (16) supplemented by reflective and absorbing boundary conditions $\tau_c'(0) = 0$ and $\tau(s) = 0$ [22]. Proceeding as in Sec. V, we find again the expression:

$$\tau_c(x_0) = 2N \int_{x_0}^s dy e^{-N\phi(y)} \int_0^y \frac{e^{N\phi(v)} dv}{T^+(v) + T^-(v)}, \quad (26)$$

with $\phi(v) = -2 \int_0^v du \left\{ \frac{T^-(u) - T^+(u)}{T^-(u) + T^+(u)} \right\}$. As shown in the inset of Fig. 10, this expression is in good agreement with the results of stochastic simulations and captures the functional dependence of the MCT whose leading contribution grows logarithmically with N and increases with q . It is also worth noting that Eq. (26) also provides a meaningful approximation of the MCT in the metastable regime, even though when $N \gg 1$ its predictions are usually less accurate than those of the WKB method, see *e.g.* [28, 30].

VII. SUMMARY AND CONCLUSION

We have studied the dynamics of the non-linear q -voter model (q VM) in the presence of inflexible zealots in a finite well-mixed population. In this model, voters can support two parties and are either “susceptibles” or “inflexible zealots”. Susceptible voters adopt the opinion of a group of $q \geq 2$ neighbors if they all agree, while zealots are here individuals whose state never changes. The q VM with zealots is introduced as a simple non-trivial model able to capture the essence of important concepts of social psychology and sociology, such as the relevance of conformity and independence as mechanisms for collective social actions [5, 6], and the existence of group-size

threshold that greatly influences the social impact of conformity [7].

In spite of its simplicity and the fact that the detailed balance is satisfied, the dynamics of the non-linear q VM with zealots is rich and characterized by fluctuation-driven phenomena and non-trivial probability distributions. The dynamics is particularly interesting at low level of zealotry, when the stationary distribution is bimodal. In this case, we have found that when one party has more zealots than the other, the intensity of one peak greatly exceeds that of the other. The dynamics is thus characterized by various time scales and growing fluctuations around a state in which a majority of susceptibles support the party having more zealots. When both parties have the same number of zealots, below the critical zealotry, the long-time dynamics is characterized by the susceptibles endlessly swinging from a state in which they all support one party to the state where they all support the other party. We have rationalized all these features

by computing the exact stationary probability distribution and, within the backward Fokker-Planck formalism, the mean times for all susceptibles to switch allegiance. We have thus found that these mean switching times grow approximately exponentially with the population size, and they increase when the number of zealot decreases at low zealotry. When zealots support only one party, we have shown that a consensus is reached in a mean time that grows either exponentially or logarithmically with the population size, depending on the zealotry density and the initial condition.

Our findings show that the properties of the non-linear q VM with zealots ($q \geq 2$) are dominated by fluctuations, and have revealed that they are sensitive to even a small bias in the zealot densities. Most of the features of the non-linear q VM with inflexible zealots are therefore beyond the reach of a simple mean field analysis and generally deviate from those of the classical linear voter model.

-
- [1] T. M. Liggett, *Interacting Particle Systems* (Springer, U.S.A., 1985).
- [2] C. Castellano, S. Fortunato, and V. Loreto, *Rev. Mod. Phys.* **81**, 591 (2009).
- [3] S. Galam, *Sociophysics* (Springer, Berlin, 2012); P. Sen and B. K. Chakrabarti, *Sociophysics: An Introduction* (Oxford University Press, Oxford, 2013).
- [4] R. J. Glauber, *J. Math. Phys.* **4**, 294 (1963).
- [5] M. Granovetter, *Am. J. Sociol.* **83**, 1420 (1978).
- [6] B. Lattané, *Am. Psychologist* **36**, 343 (1981); P. Nail, G. MacDonald, and D. Levy, *Psych. Bull.* **126**, 454 (2000).
- [7] S. E. Asch, *Scientific American*, **193**, 35 (1955); S. Milgram, L. Bickman, and L. Berkowitz, *J. of Personality and Soc. Psychology* **13**, 79 (1969).
- [8] M. Mobilia, *Phys. Rev. Lett.* **91**, 028701 (2003).
- [9] M. Mobilia and I. T. Georgiev, *Phys. Rev. E* **71**, 046102 (2005).
- [10] M. Mobilia, A. Petersen, and S. Redner, *J. Stat. Mech.* **P08029** (2007).
- [11] M. Mobilia, *J. Stat. Phys.* **151**, 69 (2013).
- [12] S. Galam and F. Jacobs, *Physica A* **381**, 366 (2007); K. Sznajd-Weron, M. Tabiszewski, and A. M. Timpanaro, **96**, 48002 (2011). D. Acemoglu *et al.*, *Math. Op. Res.* **38**, 1 (2013); P. Nyczka and K. Sznajd-Weron, *J. Stat Phys.* **151**, 174 (2013); E. Yildiz *et al.*, *ACM Transactions on Economics and Computation* **1**, 19:1 (2013); F. Palombi and S. Toti, *J. Stat Phys.* **156**, 336 (2014); A. Waagen *et al.*, *Phys. Rev. E* **91**, 022811 (2015); D. L. Arendt and L. M. Blaha, *Comput. Math. Organ. Theory* **21**, 184 (2015); N. Masuda, *New J. Phys.* **17**, 033031 (2015).
- [13] J. Xie *et al.*, *Phys. Rev. E* **84** 011130 (2011); N. Masuda, *Scientific Reports* **2**, 646 (2012); G. Verma, A. Swami, and K. Chan, *Physica A* **395**, 310 (2014); C. Borile *et al.*, *J. Stat. Mech.* **P01030** (2015).
- [14] C. Castellano, M. A. Munoz, and R. Pastor-Satorras, *Phys. Rev. E* **80**, 041129 (2009).
- [15] K. Sznajd-Weron and J. Sznajd, *Int. J. Mod. Phys. C* **11**, 1157 (2000).
- [16] F. Slanina and H. Lavicka, *Eur. Phys. J. B* **35**, 279 (2003).
- [17] P. Nyczka, K. Sznajd-Weron, and J. Cislo, *Physica A* **391**, 317 (2012).
- [18] R. Lambiotte and S. Redner, *EPL* **82**, 18007 (2008).
- [19] F. Slanina, K. Sznajd-Weron, and P. Przybyla, *EPL* **82**, 18006 (2008); S. Galam and A. C. R. Martins, *EPL* **95**, 48005 (2011).
- [20] P. Przybyla, K. Sznajd-Weron, and M. Tabiszewski, *Phys. Rev. E* **84**, 031117 (2011); A. M. Timpanaro and C. P. C. Prado, *Phys. Rev. E* **89**, 052808 (2014); A. M. Timpanaro and S. Galam, e-print: arXiv:1408.2734v1.
- [21] In the formulation of Ref. [14], the agent can still change its opinion with a probability ϵ , even if not all its q neighbors agree. For simplicity, here we have $\epsilon = 0$ as in [20].
- [22] N. G. Van Kampen, *Stochastic Processes in Physics and Chemistry* (Elsevier, NY, 2007); C. Gardiner, *Stochastic Methods* (Springer, NY, 2010); S Redner, *A Guide to First-Passage Processes* (Cambridge University Press, NY, 2001); H. Risken, *The Fokker-Planck Equation* (Springer, Berlin, 1996).
- [23] D. T. Gillespie, *J. Comput. Phys.* **22**, 403 (1976).
- [24] S. H. Strogatz, *Nonlinear Dynamics and Chaos* (Westview Press, Cambridge, MA, 1994).
- [25] P. Hänggi, P. Talkner, and M. Borkovec, *Rev. Mod. Phys.* **62**, 251 (1990).
- [26] G. B. Arfken and H. J. Weber, *Stochastic Methods* (Academic Press, San Diego, 2001).
- [27] H. Eyring, *J. Chem. Phys.* **3**, 107 (1935); H. A. Kramers, *Physica* **7**, 284 (1940).
- [28] M. Mobilia and M. Assaf, *EPL* **91**, 10002 (2010); M. Assaf and M. Mobilia, *J. Stat. Mech.* **P09009** (2010); M. Assaf and M. Mobilia, *J. Theor. Biol.* **275**, 93 (2011); M. Mobilia, *J. Stat. Phys.* **151**, 69 (2013).
- [29] L. D. Landau and E. M. Lifshitz, "Quantum Mechanics: Non-Relativistic Theory" (Pergamon, London, 1977); M. I. Dykman *et al.*, *J. Chem. Phys.* **100**, 5735 (1994).
- [30] M. Assaf and B. Meerson, *Phys. Rev. E*, **75**, 031122 (2007); *Phys. Rev. E* **81**, 021116 (2010); C. Escudero and A. Kamenev, *Phys. Rev. E* **79**, 041149 (2009).